This is a repository copy of *Electrical and Magnetic Properties of NiZn Ferrite Prepared by Conventional and Solar Sintering*.

White Rose Research Online URL for this paper:
http://eprints.whiterose.ac.uk/99070/

Version: Accepted Version

Electrical and magnetic properties of NiZn ferrite prepared by conventional and solar sintering

Jesús Gutiérrez-López[1], Nahum Masó[2], Belen Levenfeld[1], Alejandro Várez[1], Anthony R. West[2]

[1] Department of Materials Science and Engineering, Universidad Carlos III de Madrid. Avda. Universidad, 30. 28911-Leganés, Spain

[2] Department of Materials Science and Engineering, University of Sheffield, Mappin Street, Sheffield, S1 3JD, United Kingdom

Abstract

The electrical properties of polycrystalline NiZn ferrite, $Zn_{0.44}Ni_{0.38}Fe_{2.18}O_4$, were investigated by impedance spectroscopy over the frequency and temperature ranges, 5 Hz to 2 MHz and 10 to 600 K and by magnetic permeability measurements at room temperature. Samples were sintered in either conventional or solar furnaces followed by quenching or slow cooling to ambient temperature. Depending on processing conditions, the room temperature electrical resistivity of conventionally-sintered samples varied by seven orders of magnitude, from 5 ohm cm for a sample quenched from 1250 ^{o}C to 10 Mohm cm for a sample quenched from 400 ^{o}C; corresponding activation energies varied from 0.005 to 0.437 eV. These variations were attributed to the oxygen content of the ferrite which decreased with increasing temperature and in oxygen-deficient samples, led to mixed oxidation state of Fe in the octahedral B sites of the spinel structure. Samples sintered in the solar furnace were much more conductive than ones that were slow-cooled after conventional sintering and this is attributed to the relatively rapid cooling rate after exposure in the solar furnace, which preserved some of the oxygen deficiency present at high temperature. For the same reason, samples that were slow cooled in N_2 were also much more conductive. For conventionally-sintered samples of similar density, quenched samples had much higher imaginary permeability, attributed to their lower resistivity and higher eddy currents, than slow-cooled samples. Solar-sintered samples had higher real permeability than slow-cooled, conventionally-sintered ones mainly due to a combination of their lower resistivity and higher density, 96% compared to 86%.

1   Introduction

Ferrimagnetic materials, such as ferrites, are widely used as core material for power transformers and in high frequency devices. An important property of these materials is their high electrical resistance which, compared with that of other magnetic materials, greatly reduces eddy current losses at high frequencies[1]. The influence of additives[2], grain size and grain size distribution[3], sintering time[4], temperature[5] and Ni,Zn:Fe ratio[6] on the electrical properties of ferrites have been widely studied. However, there are no reported studies on the specific effect of possible oxygen non-stoichiometry, and its dependence on cooling rate from high temperature, on the electrical properties.

Impedance spectroscopy, IS, is an invaluable, non-destructive tool for analyzing the electrical properties of functional ceramics[7]. Using IS, it is possible to separate the bulk and grain boundary contributions to total conductivity[8]. A few studies on the characterization of ferrites using this technique have been reported[1,9,10,11]. In those studies, in air, the ferrites were clearly heterogeneous electrically and were characterised by low resistivity grains separated by high resistivity grain boundaries.

Use of a solar furnace for sintering offers the possibility of fast sintering due to its ability to reach high temperatures in short times, with heating/cooling rates up to several tens of degrees per minute. It is also a powerful and environmentally-friendly technique with no associated CO_2 emissions. Previous work has demonstrated the applicability of solar sintering to the densification of ceramic powder such as cordierite-based ceramics[12], Si_3N_4[13] and alumina[14].

Recently, we investigated the solar sintering of commercial Ni-Zn ferrite powders; the mechanical and magnetic properties were compared with those of similar material sintered in a conventional electrical furnace[15]. Suitable sintering conditions with the solar furnace were found to be a sintering temperature of 1250 ^{o}C for 30 mins in air using a heating / cooling rate of 30 ^{o}Cmin^{-1}. Preliminary studies on conventionally-sintered samples showed that the cooling rate after sintering may have a dramatic effect on the subsequent electrical properties. Here, we therefore report a systematic study of the effect of annealing temperature and cooling rate on the electrical and

magnetic properties of well-sintered Ni,Zn ferrites obtained by both conventional and solar sintering and demonstrate clear correlations between sample processing conditions, electrical conductivity and magnetic permeability.

2   Experimental Procedure

2.1   *Materials*

The starting raw material was a granulated pre-sintered Ni-Zn ferrite ($Zn_{0.44}Ni_{0.38}Fe_{2.18}O_4$) powder that is typically used for the industrial manufacturing of ferrites. The powder was a presintered mixture of Fe_2O_3, NiO and ZnO provided by Ferroxcube which was heavily agglomerated (30-300 μm) into large spheres as a consequence of its preparation by spray-drying. During this powder conditioning, about 1-2 weight % of organic component was incorporated into the powders.

2.2   *Processing and experimental techniques*

Green specimens were fabricated by uniaxial compaction using a dual effect press and 100 MPa of pressure (standard industrial conditions) in the form of toroids, 10.3 mm outer diameter x 5 mm inner diameter x 3.45 mm depth.

One batch of samples was sintered in air in a conventional furnace at 1250 ºC for 2 hours and cooled at 3.5 ºC/min. Some of these samples were then heated at 1250 ºC and cooled rapidly (approx. 100 ^{o}Csec^{-1}) by quenching into liquid nitrogen.

A second batch of samples was sintered in a solar furnace at 1250 ºC for 30 mins in air using a heating/cooling rate of 30 ºC/min. These experiments were carried out in the Solar Furnace (SF60) of the Plataforma Solar de Almería (PSA-CIEMAT) in Spain. The operating conditions of the solar furnace have been described by Román *et al*[14]. This solar system essentially consists of a continuous solar-tracking flat heliostat, a parabolic concentrator mirror (collector), an attenuator (shutter) and a test zone located in the concentrator focus centre.

The temperature in the solar furnace was managed by the opening of the shutter. When the shutter is 100% open and the system is illuminated at a direct solar irradiance of 1000 W/m^2, the focus is

characterised to have an irradiance peak of 3051 kW/m^2 and a total power of 68 kW[16]. The temperature in the central part of the chamber, where samples are located, is controlled by an alumina-protected thermocouple. Furthermore, an infrared camera is used to monitor a profile of the relative temperature distribution along the chamber surface. In figure 1, the temperature profile of the thermocouple and IR camera during the experiment is displayed. The opening of the shutter (in %) is also plotted.

In order to control the temperature of the samples, 4 sintering rings (Ferro electronic materials, PTCR-STH 214) were used as shown in figure 2. After sintering, the diameter of these rings, calibrated against coefficient of thermal expansion data, was measured to ascertain the temperature achieved in the furnace.

Slow-cooled and quenched samples were analyzed by X-ray powder diffraction, XRD using a STOE STADI P diffractometer with Mo Kα_1 radiation (λ = 0.7092 Å) and Si as external standard for d-space measurements. Indexing of the XRD patterns was carried out using WinXPow software. The sintered densities were determined using the Archimedes method.

For electrical property measurements, samples, with gold electrodes sputtered on opposite faces, were attached to the Pt leads of a conductivity jig and, for measurements above room temperature, placed inside a non-inductively wound horizontal tube furnace with temperature controlled and measured to within 3º. For measurements between 10 K and room temperature, the jig was placed inside a cryocooler. Two impedance instruments were used, both with a small applied ac voltage, nominally 100 mV: an HP impedance analyzer 4192A over the frequency range 5 Hz to 10 MHz, with the added facility to take measurements at the same time as application of a *dc* bias and an Agilent E4980A Precision LCR meter over the frequency range 25 Hz to 2 MHz. All impedance measurements were carried out in air.

The real, µ' and imaginary, µ'' parts of the magnetic permeability were measured as a function of frequency at room temperature with a Hewlett-Packard LCR-meter HP4285A over the frequency range 100 kHz to 11.5 MHz.

3   Results and discussion

XRD patterns of slow-cooled and quenched samples are shown in figure 3. Both samples were single phase with spinel structure. The lattice parameters, determined by Rietveld analysis, were similar: 8.3925(5) Å and 8.4054(2) Å for slow-cooled and quenched samples, respectively. The slightly larger value for the quenched sample is attributed to a small, but unquantified amount of oxygen loss at high temperature which was preserved by quenching. Although lattice contraction might be expected as a result of the loss of some large oxide anions from the structure, this is more than offset by the reduction in average ionic bond strength associated with oxygen loss: O_2 gas is liberated, electrons are injected into the structure, the average positive charge on the transition metal components reduces and there are fewer negatively-charged anions present in the structure. Consequently, a lattice expansion occurs.

The density of conventionally-sintered, slow-cooled and quenched samples was 87% of the theoretical value while solar-sintered samples were 96% dense[15]. SEM micrographs of slow-cooled, solar-sintered and quenched samples are shown in figure 4. Similar microstructures are seen in slow-cooled and quenched samples with a small grain size, while solar-sintered ferrites have a bimodal distribution with grains of approximately 20 μm and 3 μm size.

A typical impedance data set for conventionally-sintered, slow-cooled samples is shown in figure 5. Data are presented in the form of impedance complex plane plots, Z" / Z' (a), as Z", M" spectroscopic plots (b) and as C' spectroscopic plots (c). Impedance data are corrected for overall sample geometry and are reported in units of ohm cm. Values of bulk resistance therefore approximate to resistivity values but the grain boundary values do not since they are not corrected for the geometry of the grain boundary regions. We therefore refer to data as resistances, although the units are given as ohm cm. Two arcs are shown in the impedance complex plane at 414K and 437K, one at high frequency with low resistance and the other at low frequency with a somewhat higher resistance. The Z"/M" spectroscopic plots show two peaks in the case of Z" but only one in M" which overlaps with the higher frequency of the two Z" peaks. The C' spectrum shows a high frequency plateau and a low frequency plateau.

All data were consistent with an equivalent circuit consisting, ideally, of two parallel RC elements connected in series. Z* data show well-defined arcs and resistance values were extracted directly from intercepts on the real, Z' axis; detailed circuit fitting has not been carried out. Such a circuit gives, as shown in figure 5, two arcs in the impedance complex plane, A, two peaks in the Z" spectrum, B, one or two peaks in the M" spectrum depending on the magnitudes of the associated capacitances, B and two plateaux in the C' spectroscopic plot, C.

The high frequency plateau has capacitance $\approx$ 4 pFcm^{-1} which is a typical value for a bulk capacitance[8]. The low frequency value, around 1 nFcm^{-1}, is typical for a grain boundary impedance. The low frequency C' plateau is associated with the larger, low frequency arc in the impedance complex plane and the low frequency peak in the Z" spectrum, while the high frequency plateau is associated with the high frequency impedance arc and the M" peak. A second, low frequency M" peak is present but is not apparent on the linear M" scale used in figure 5: M" peak heights are inversely proportional to capacitance and the grain boundary capacitance is approximately 250 times larger than the grain capacitance.

The resistivity of the grain boundary is several orders of magnitude higher than that of the grains. From the ratio of the capacitance data, and assuming (i) a series connection of grains and grain boundaries and (ii) the grains and grain boundaries have the same permittivity, the thickness of the grain boundaries is estimated to be only ~0.25 % of that of the grains. Such data are typical of many electroceramics that show both bulk and grain boundary contributions to the overall impedance and for which a series equivalent circuit is appropriate.

Impedance data for solar-sintered samples are similar in general appearance to those of the slow-cooled samples but appear in the measuring frequency range only at much lower temperatures. Thus, two semicircles are seen in impedance complex plane plots at 10 and 20 K, figure 6 and two plateaux are observed in C' spectroscopic plots. The resistances of the solar-sintered sample are very much less than those of the slow-cooled sample and are attributed to the higher conductivity associated with oxygen-deficiency of the solar-sintered samples.

Impedance data for a conventionally-sintered sample quenched from 1250 ^{o}C are shown in figure 7. Low measuring temperatures were necessary for impedance data to be accessible over the frequency range of the instrumentation, but there was one notable difference to the solar-sintered sample data: the C' spectroscopic plot shows evidence of a third, poorly-resolved, low frequency plateau at approximately 10 nFcm^{-1} and the impedance complex plane plots show a third, low frequency arc. Capacitance values of this magnitude are usually associated with sample surfaces[8] or sample-electrode interfaces[17].

A useful test to gain further information on the origin of the various impedances that are detected is to carry out impedance measurements with / without an applied *dc* bias. Results are presented in figure 8 which show that the third, lowest frequency arc in the complex plane plot decreases in size with increasing *dc* bias and is largely absent with 5 V bias. This indicates that the third arc is a potential barrier impedance, rather than a material impedance and is attributed to formation of a Schottky barrier[17] at the sample-electrode interface, associated with a mismatch in Fermi levels across the interface. In order for Schottky barriers to be detected readily in impedance data, it is usually necessary that their associated resistances are comparable to or greater than those of other resistances within the sample.

As a first step in the creation of a Schottky barrier, a significant amount of electron spill-over occurs between the metal electrode and the quenched sample, leading to a space charge layer at the sample surface whose resistive properties are different to those of the sample interior. For the quenched samples, the bulk and grain boundary resistances are several orders of magnitude less than those of slow-cooled samples. Schottky barriers form spontaneously at the electrode-sample interfaces and the barrier height can be reduced on application of a *dc* bias, as shown in figure 8.

The large difference in electrical properties between, on the one hand, slow-cooled samples and on the other hand, solar-sintered samples and especially, quenched samples, is attributed to a small, unquantified, amount of reversible oxygen loss from the ferrite samples at high temperature. Many oxides start to lose oxygen at high temperatures and the electrons that are released, by the mechanism:

$$O_O^x \Leftrightarrow 1/2 O_2 + 2e' + v_o^{\bullet\bullet} \qquad\qquad (1)$$
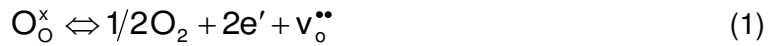
can give rise to dramatic increases in the electronic conductivity. An excellent example is rutile which changes from an insulator in slow-cooled samples to a good semiconductor in samples quenched from eg 1200 ^{o}C, even though the amount of oxygen loss was barely detectable by weight loss studies[17]. We suggest that the Ni,Zn ferrite samples may also lose oxygen at high temperatures; if the samples are quenched, the oxygen non-stoichiometry is retained, but if they are slow-cooled, reoxidation occurs. Comparison of the electrical properties of the different samples indicates that the solar-sintered sample may have a significant degree of oxygen deficiency, but not as much as that in the quenched samples. Some reoxidation occurred during cooling in the solar furnace, therefore, but was incomplete, perhaps due to a combination of the relatively fast cooling rate and the reduced porosity of the solar-sintered samples

Oxygen loss under equilibrium conditions generally increases increasingly rapidly with temperature and can be studied by quenching samples from different temperatures after equilibration. On measuring their electrical conductivity at room temperature, the high temperature condition is effectively frozen-in. Results are shown in figure 9 for the total conductivity of materials quenched from temperatures in the range 400 to 1250 ^{o}C. The room temperature resistivity decreases by almost 7 orders of magnitude with increasing quench temperature. A similar large change was observed by van Uitert[6] but was associated with variation of the Ni,Zn:Fe ratio. In addition to possible oxygen loss, the volatilization of Zn at high temperature was suggested as an additional mechanism by which the composition may vary during sintering of NiZn ferrites[6]. However, it was reported that Zn losses are negligible for sintering above 1250 ^{o}C[18]. Furthermore, from our results shown in figure 3, the XRD patterns and refined lattice parameters are similar and may indicate little change in cationic composition on firing at 1250 ^{o}C.

The decrease in resistivity is attributable to the formation of Fe^{2+}. The formation of Fe^{2+} allows electron hopping between Fe^{2+} and Fe^{3+} ions which brings about a reduction in resistivity[19]. Further work is required to (i) quantify the oxygen non-stoichiometry as a function of temperature and (ii) determine whether volatilization of Zn leads to a modification in cation composition and

conductivity of samples sintered in the solar furnace and in samples subjected to similar thermal treatments.

Arrhenius plots of the bulk conductivity of the three main categories of sample are shown in figure 10. The slow-cooled sample gives an approximately linear plot with activation energy, 0.44 eV. This value is slightly higher than those (0.1-0.4 eV) reported for Ni-Zn ferrites prepared by conventional dry solid-state reaction[20] and slightly lower than samples synthesized by a wet-chemical method (0.55-0.73 eV) and is dependent on the sintering conditions and/or Zn losses. The quenched and solar-sintered samples show non-linear plots with a tendency to very low activation energy at low temperatures. We attribute the non-linear Arrhenius plots of the samples that were not fully oxidized to a transition from extrinsic to intrinsic behavior with increasing temperature. These samples were oxygen-deficient to a certain, but unknown, extent and the electrons liberated on oxygen loss were presumably located on Fe as Fe^{2+}. The low activation energy at low temperatures, below ~20 K, is attributed to easy electron hopping between Fe^{2+} and Fe^{3+}. The conductivity of the quenched sample is higher than that of the solar-sintered sample, consistent with the expectation that the quenched sample is more reduced and therefore, has a higher carrier concentration.

At higher temperatures, all three samples have much higher activation energy for conduction; most of this activation energy is associated with an additional carrier creation process, the details of which are unclear. But, if it is assumed that Fe in the fully oxidized, slow-cooled sample is entirely Fe^{3+}, then presumably, electron promotion to higher levels within Fe^{3+} occurs, leading to the region of intrinsic conductivity.

Real and imaginary parts of the permeability at room temperature for the three categories of sample are shown in the figure 11; all samples show a similar behavior. At low frequency, the real permeability, µ′, is constant over several decades of frequency until a certain frequency is reached at which the permeability reaches a maximum value, especially for slow-cooled samples and afterwards shows a significant decrease. The fairly constant µ′ values over a large frequency range show the compositional stability and quality of the ferrites prepared. This flat region, known as the *zone of utility* of the ferrite, is a desirable characteristic for various applications such as broadband

pulse transformers and wideband read-write heads for video recording. Solar-sintered samples have higher permeability than slow-cooled samples; this may be associated with a significant increase in density[21] (96 % of theoretical density for solar-sintered samples vs 86 % for slow-cooled specimens), but the grain size of the solar samples is also significantly greater, which may indicate a correlation between grain size and permeability[22]. Quenched and slow-cooled samples have similar density but different permeability which may indicate a correlation between resistivity and permeability. Hence, several sample variables: density/porosity, grain size/size distribution and resistivity, may all have an influence on the real permittivity.

The imaginary part of the permeability, μ'', decreases with increasing frequency, passes through a minimum and then increases to a maximum; this is not a sharp maximum, as would be expected for a resonant frequency, but is more indicative of either a distribution of resonant frequencies or a relaxation frequency. Slow-cooled samples have the lowest imaginary permeability, independent of density while quenched samples have the highest value. This may be because quenched samples have low resistivity and therefore, high eddy currents[6]. These results show that resistivity appears to have a greater correlation with the imaginary permeability than has density.

4   Conclusions

Impedance spectroscopy has shown two contributions to the impedance of NiZn ferrites, a higher resistivity grain boundary and a lower resistivity bulk for both conventionally-sintered and solar-sintered ferrites. In addition, for highly conducting quenched samples, a third resistance was attributed to Schottky barriers which were removed by application of a dc bias. A strong correlation between cooling rate and electrical properties of NiZn ferrites has been demonstrated. Higher cooling rates associated with quenching cause an increase in electrical conductivity by almost 7 orders of magnitude. This is attributed to a small amount of unquantified oxygen loss at high temperatures which is likely to be regained at slower cooling rates. Using a solar furnace with a cooling rate of 30 ºC/min, the electrical conductivity was intermediate between that of slow-cooled and quenched samples and was attributed to partial reoxidation during cooling. Conductivity

Arrhenius plots of oxygen-deficient samples show a change from low activation energy, extrinsic conduction at low temperature, associated with electron hopping between Fe^{2+} and Fe^{3+}, and intrinsic conduction with activation energy 0.44 eV at high temperature.

.The magnetic properties revealed the importance of the different sample processing variables. ~~On the one hand,~~ Solar-sintered samples have the highest real permeability, µ', because of their high density and/or grain size/size distribution. On the other hand, a slow cooling rate leads to a lower imaginary permeability, µ″, due to increased oxygen content and a higher electrical resistivity. Resistivity can also modulate the real permeability for samples with similar density and grain size.

References

[1] J. T. S. Irvine, A. Huanosta, R. Valenzuela, A. R. West. "Electrical properties of polycrystalline Nickel Zinc Ferrites," *J. Am. Ceram. Soc.*, **73** [3] 729-732 (1990).

[2] S-F Wang, Y-R Wang, T. C. K. Yang, C-F Chen, C-A Lu, C-Y Huang. "Densification and magnetic properties of low-fire NiCuZn ferrite," *J. Magn. Magn. Mater,.* **220** [2-3]129-138 (2000).

[3] R. Valenzuela. "Caracterización de materiales por espectroscopia de impedancias" *Revista cubana de física.,* **19** [2] 81-84 (2002).

[4] B. P. Rao, K. H. Rao, "Effect of sintering conditions on resistivity and dielectric properties of Ni-Zn ferrites" *J. Mater. Sci.,* **32** [22] 6049-6054 (1997).

[5] T. Jahanbin, M. Hashim, K. A. Matori, S. B. Waje. "Influence of sintering temperature on the structural, magnetic and dielectric properties of $Ni_{0.8}Zn_{0.2}Fe_2O_4$ synthesized by co-precipitation route," *J. Alloy Compd.,* **503** [1] 111-117 (2010).

[6] L. G. Van Uitert "DC resistivity in the Nickel and Nickel Zinc Ferrite system," *J. Chem. Phy.,* **23** [10] 1883-1887 (1955).

[7] J. R. MacDonald, E. Barsoukov. "*Impedance spectroscopy: Theory, experiment and applications*" Wiley Interscience. John Wiley & Sons, Inc., Hoboken, New Jersey, 2005.

[8] J. T. S. Irvine, D. C. Sinclair, A. R. West. "Electroceramics: Characterization by Impedance Spectroscopy," *Adv. Mater.* **2** [3] 132-138 (1990).

[9] N. Sivakumar, A. Narayanasamy, N. Ponpandian, J-M Greneche, K. Shinoda, B. Jeyadevan, K. Tohji. "Effect of mechanical milling on the electrical and magnetic properties of nanostructured $Ni_{0.5}Zn_{0.5}Fe_2O_4$," *J. Phys. D Appl. Phys.,* **39** [21] 4688-4694 (2006).

[10] H-F Cheng. "Modeling of electrical response for semiconducting ferrite," *J. Appl. Phys.* **56** [6] 1831-1837 (1984).

[11] R. C. Kambale, P. A. Shaikh, C. H. Bhosale, K. Y. Rajpure, Y. D. Kolekar. "Dielectric properties and complex impedance spectroscopy studies of mixed Ni-Co ferrites" *Smart Mater. Struct.*, **18** 1-6 (2009).

[12] F. Oliveira, L. Guerra-Rosa, J. Fernandes, J. Rodriguez, I. Cañadas, D. Martinez, N. Shohoji. "Mechanical properties of dense cordierite discs sintered by solar radiation heating," *Mater. Trans.* **50** [9] 2221-2228 (2009).

[13] N. Zhilinska, I. Zalite, J. Rodríguez, D. Martínez, I. Cañadas. "Sintering of nanodisperse powders in a solar furnace," pp. 423-428, Vol. 3, in *Proceeding of the Euro PM2003 Conference.* 2003 ,

[14] R. Román, I. Cañadas, J. Rodríguez, M. T. Hernández, M. González. "Solar sintering of alumina ceramics: Microstructural development," *Solar Energy.,* **82** [10] 893-902 (2008).

[15] J. Gutiérrez-López, B. Levenfeld, A. Varez, J. Y. Pastor, I. Cañadas, J. Rodriguez. "Study of densification, mechanical and magnetic properties of Ni-Zn ferrites sintered in a solar furnace," *Ceram. Int*, **41** [5] 6534-6541 (2015).

[16] J. Rodríguez, I. Cañadas, J. Fernández, R. Monterreal, J. Ballestrín, F. Téllez, L. Yebra "The PSA Solar Furnace, a test facility ready to characterize high-concentration solar devices from solar thermal applications to PV cells," pp. 20-23, in *Proceedings of 13th International Symposium on Concentrated Solar Power and Chemical Energy Technologies*. Seville, Spain, 2006.

[17] Y. Liu, A.R. West, "Semiconductivity-insulator transition in undoped rutile, TiO_2 ceramics," *J. Amer. Ceram. Soc.*, **96** [1] 218-222 (2013).

[18] A. Verma, R. Chatterjee. "Effect of zinc concentration on the structural, electrical and magnetic properties of mixed Mn-Zn and Ni-Zn ferrites synthesized by citrate precursor technique," *J. Magn. Magn. Mater.,* **306** [2] 313-320 (2006).

[19] E.J.W. Verwey, J.H. de Boer. "Cation arrangement in a few oxides with crystal structures of the spinel type," *Rec. Trav. Chim. Pays-Bas*, 55 [6] 531-540 (1936); and A. Verma, T.C. Goel, R.G. Mendiratta and R.G. Gupta "High-resistivity nickel–zinc ferrites by the citrate precursor method", *J. Magn. Magn. Mater.,* **192**, [2] 271-276 (1999).

[20] A. Verma O.P. Thakur, C. Prakash, T.C. Goel, R.G. Mendiratta, "Temperature dependence of electrical properties of nickel-zinc ferrites processed by the citrate precursor technique", *Mat. Sci. Eng. B*, **116**, 1-6 (2005), and references therein cited.

[21] A. Goldman. *Modern Ferrite Technology.* Springer, Pittsburgh, PA. USA, 2006.

[22] A. Globus and P. Duplex. "Separation of susceptibility mechanims for ferrites of low anisotropy", *IEEE Trans. Magn.,* **2** [3] 441-445 (1966).

[21] J. L. Snoek. "Dispersion and absorption in magnetic ferrites at frequencies above one Mc/s," *Physica,* 14 [4] 207-217 (1948).

Figure Captions

Fig.1 Variation of temperature measured by: thermocouple; infrared camera; opening of the shutter.

Fig. 2 Sintering rings (white) to determine the maximum temperature of ferrites (brown) achieved in the solar furnace

Fig. 3 XRD patterns of NiZn ferrite quenched from 1250ºC and slow-cooled, with Mo Kα_1 radiation, $\lambda = 0.7092$ Å

Fig. 4 SEM micrographs of slow-cooled (left), solar-sintered (centre) and quenched samples (right) sintered at 1250 ºC

Fig. 5 Typical IS data sets measured at 414 K and 437 K of slow-cooled NiZn ferrite (a) impedance complex plane (b) Z'', M'' spectroscopic plots and (c) C' spectroscopic plots.

Fig. 6 IS data measured at 10 and 20 K of NiZn ferrites sintered in a solar furnace; (a) impedance complex plane plots, (b) C' spectroscopic plots.

Fig. 7 IS data measured at 10 and 20 K of quenched NiZn ferrites (a) impedance complex plane (b) C' spectroscopic plot.

Fig. 8 Effect of dc bias on the impedance complex plane plots of a quenched NiZn ferrite measured at 10K

Fig. 9 Resistivity of NiZn ferrite as a function of quench temperature.

Fig. 10 Arrhenius plots of total resistivity emphasizing (a) high and (b) low temperature data.

Fig. 11 Real (continuous line) and imaginary (dashed line) parts of permeability as a function of frequency at room temperature.